First Steps towards a Roboticized Visual Inspection System for Vessels*

A. Ortiz, F. Bonnin
University of Balearic Islands
Palma de Mallorca - Spain
alberto.ortiz@uib.es

A. Gibbins, P. Apostolopoulou
W. Bateman - Lloyd's Register
London - UK
Andrew.Gibbins@lr.org

M. Eich
DFKI
Bremen - Germany
markus.eich@dfki.de

F. Spadoni
RIGEL Engineering S.p.A.
Livorno - Italy
spadoni@rigel.li.it

M. Caccia
CNR-ISSIA
Genova - Italy
max@ge.issia.cnr.it

L. Drikos
Glafcos Marine
Piraeus - Greece
leodrikos@glafcos-marine.com

Abstract

Vessel maintenance entails periodic visual inspections of internal and external parts of the vessel hull in order to detect the typical defective situations affecting metallic structures, such as cracks, corrosion, etc. This paper presents the first steps towards a roboticized visual inspection system aiming at automating as much as possible the whole inspection process currently undertaken by human surveyors. Occurrence of defects are first outlined, followed by a brief description of the whole system. Next, details for one of the robotic platforms to be used are given, as well as for the image processing algorithms dealing with the visual detection of defects.

1. Introduction

The movement of goods by ships is today one of the most time and cost effective methods of transportation. The safety of these vessels is overseen by the classification societies, who are continually seeking to improve standards and reduce the risk of maritime accidents. Structural failures are a major cause of accidents, and can usually be prevented through timely maintenance. As such, vessels undergo annual inspections, with intensive Special and Docking Surveys every five years, which ensures that the hull structure and related piping are all in satisfactory condition and are fit for the intended use over the next five years.

To illustrate the enormity of the inspection task, the surveying of a central cargo tank on a Very Large Crude Carrier (VLCC), involves checking over 860m of web frames (primary stiffening members) and approximately 3.2km of longitudinal stiffeners. Furthermore, this surveying is performed in a potentially hazardous environment with both flammable and toxic gases and signifi-

cant heights involved. As a result, while accidents are extremely rare, when they do arise they can have serious consequences. Due to these complications, the total cost of a single surveying can exceed $1M once you factor in the vessel's preparation, use of yard's facilities, cleaning, ventilation, and provision of access arrangements. In addition, the owners experience significant lost opportunity costs while the ship is inoperable.

Therefore, it is clear that any level of automation of the inspection process that can lead to a reduction of the inspection time, a reduction of the costs involved and/or an increase in the safety of the operation is fully justified. This is the main motivation for the EU FP7 project MINOAS. Indeed, MINOAS global objective is the effective virtual teleportation of the surveyor to the different areas of the vessel hull that need inspection. Contrary to similar past projects (ROTIS [5] and its follow-up ROTIS-II [1]) or commercial solutions such as [6], the scope of MINOAS comprises both dry and wet areas of the vessel, and not only flooded ballast tanks or the external hull. The MINOAS project is neither limited to tele-operated floating tethered vehicles, but considers a varied set of robotic technologies with different locomotion capabilities.

As a partial fulfilment of this general objective, this paper presents a first attempt for dealing with automated crack and corrosion detection in vessels. To this end: Section 2 discusses the cause of this kind of failures and the critical areas of the hull where they do occur; next, Sections 3 and 4 deal with the challenges of getting around the ship by means of robotic platforms so as to provide remote visual evidence of the state of the vessel hull to the surveyor; Section 5 describes image processing algorithms to assist the surveyor in the detection of cracks and corrosion; finally, Section 6 concludes the paper.

2. Analysis of defect occurrence

As with most technological developments, potential implementation is dependant on economic viability. To

Table 1. Failure analysis summary

Ship Type	Upper	Middle	Lower
Bulk carriers	53%	10%	37%
Single hull tankers	41%	30%	29%
Double hull tankers	33%	26%	41%
Average	42%	22%	36%

maximise the potential market, any development should be aimed at the most prevalent area of the world fleet, i.e. above 10,000 *deadweight tonnes* (DWT). In terms of DWT, which is indicative of the amount of material and hence the complexity of the survey, two ship types make up the lions share of the Worlds Fleet [4]: Oil tankers ($\approx$ 27%) and Bulk carriers ($\approx$ 23%).

Furthermore, to ensure the greatest potential cost saving, any developments should be focused on the areas of a ship where it has been empirically proven that the majority of failures occur. The subsequent analysis identifies theses areas and touches on the potential causes of failure in these regions. The damages considered in this paper can be generally classified as either corrosion based (excessive wastage, pitting, etc) or load based (cracks, buckling, etc).

2.1. Damage localisation

Using survey data recorded by Lloyd's Register from 1987 to 2007 it is possible to analyse the damage trends between the forward and aft cargo bulkheads of Bulk carriers, Single (SHT) and Double hull (DHT) tankers. A first pass of this data allowed localisation of damages across the top, middle and lower thirds of each vessel type. The results of this analysis, shown in Table 1, demonstrate a considerable difference between vessels, although the general trend is that the middle region experiences the fewest failures (due to the region encompassing the vessels neutral axis, hence low stresses).

While the lower regions experience significant failures, particularly within DHT, the challenges of surveying them are physically simpler compared to surveying the upper regions. Nevertheless, in order to gain access to any region of a tank, the entire tank must be cleaned, ventilated and lit. Large cost savings could be achieved if roboticized inspection systems were able to carry out full tank surveys in an unclean, low light stagnant atmosphere.

A more detailed analysis of the aforementioned data allows quantification of the damage inside individual tanks. As a result of the very different typical structures between the ship types (see Figure 1(top)), discussion on the localisation and causes of damage in each ship type will be made separately.

2.2. Damage in Bulk Carriers

Figure 1(bottom) reports on damage localisation. As can be observed, 40% of failures occur in the holds. These spaces are exposed to an extremely high degree of abuse in the form of impacts, abrasion and high localised loads, often due to unloading means. These factors not only cause material and fabrication failures, but due to the abrasion,

any applied coating is quickly rendered useless, allowing corrosion to take place.

On the other hand, Topside tanks suffer from 30% of the survey failures, which is often corrosion failure caused by the use of these tanks in ballast voyages. The cyclic filling and emptying twined with the hot and humid conditions often experienced in these tanks leads to rapid wastage, enhanced by the potential for microbial corrosion.

The Upper deck also suffers from a significant number of failures ($\approx$ 13%), potentially caused by ship bending. Additionally this region is exposed to the salt rich external corrosive atmosphere. It is important to realise that the Upper deck forms one of the tank boundaries making it possible to detect a number of defects noted on the upper deck during tank survey.

Finally, 5% of the overall damages occur in Hopper tanks. These tanks are damaged on one side by unloading actions, and on the other by a corrosive atmosphere caused by ballasting the hopper space.

2.3. Damage in Oil Tankers

The dominant mode of failure in tankers is corrosion, caused either by the cargo itself or the water from ballast voyages. In addition, tankers are not exposed to the same 'abusive' unloading as bulk carriers as the liquid cargo can be easily pumped out. However there is still a potential for material yield in certain areas due to sloshing loads. Again referring to Figure 1(bottom), Wing/Side tank failures account for over 60% of the failures in SHT, whereas only 10% of failures occur in the centre cargo tanks. This immense difference arises because some side tanks are designated for ballast and due to a combination of perhaps cheaper coatings and a corrosive atmosphere, they suffer. In DHT the Wing/ Side tanks are only used for cargo, as such the failure rate is much lower (35%). Nevertheless this is still higher than the failure in the centre tanks (16%) because they are more often partially loaded leading to larger sloshing loads and a more corrosive atmosphere.

On the other hand, the Upper decks experience relatively similar failure rates across all ship types ($\approx$ 13 − 22%) reflecting the fact that they all experience similar external conditions, while Topside tanks (found in DHT most often as part of the wing ballast tanks) suffer 8% of the total failures and are exposed to the same conditions as those seen in bulk carriers and in the wing ballast spaces. In addition, they are exposed to less severe loading in tankers as there are no large hatch openings on deck. The upper sections of the wing ballast tanks (referred to in Figure 1(bottom) as topside tanks) account for 8% of the failures in DHT. This is caused by similar conditions to those listed for bulk carriers.

Finally, Wing and double bottom ballast spaces are also prone to corrosion due to the cyclic filling and emptying. This is exacerbated by the constant changing loads applied to the tanks by the seaway itself as these tanks are partially
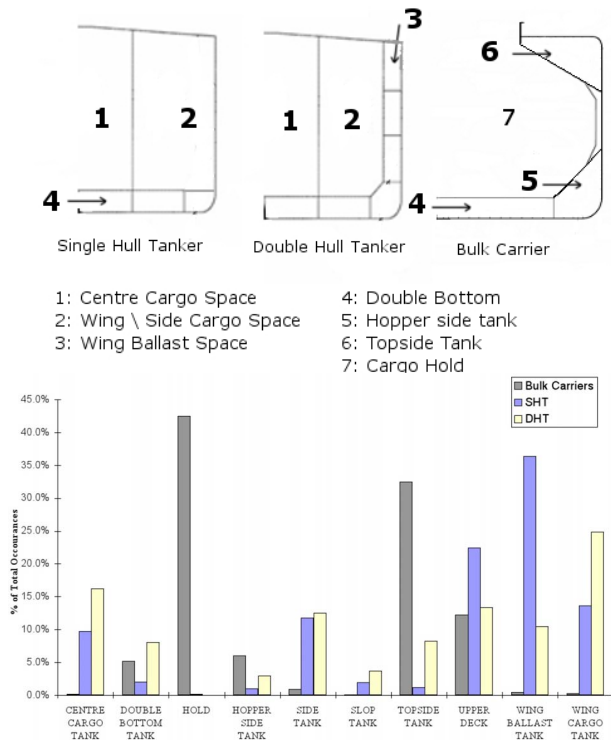
1: Centre Cargo Space
2: Wing \ Side Cargo Space
3: Wing Ballast Space
4: Double Bottom
5: Hopper side tank
6: Topside Tank
7: Cargo Hold

Figure 1. For every ship type: (top) typical sections, (bottom) damage distribution.

formed by the outer skin of the vessel.

3. Robotic infrastructure

3.1. Generalities

As already mentioned, the main goal of the MINOAS project is to allow the surveyor to be teleported to the hull parts that require inspection. To this end, and particularly from the vessel areas identified as risky in Section 2, the surveyor must be provided with:

– imagery detailed enough so as to remotely enable the visual assessment of the state of the area under inspection and also assist the surveyor before taking a "repair/no repair needed" decision with quantitative data about the extent of the defective situation; and

– thickness measurements at specific points of the hull, so as to be able to determine whether the structural integrity of the vessel is compromised.

To this end, the MINOAS project foresees the use of a robot fleet equipped with technologies that permit all relevant areas of the hull to be reached. This will include *Unmanned Aerial Vehicles* and *Wall Climbers* for effectively implementing inspection missions involving either submerged and/or non-submerged horizontal, vertical and sloped hull structures.

3.2. Outline of an inspection mission

The following stages are envisioned for a typical inspection mission:
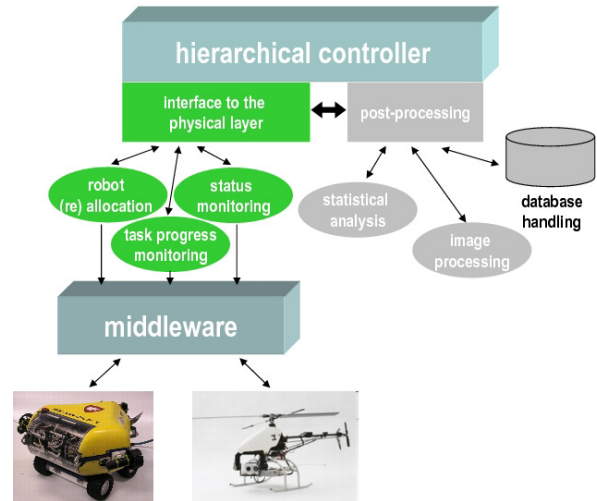

Figure 2. MINOAS architecture

– *Stage A: Video grabbing*. During this stage, the entire vessel is covered by the robot fleet and every platform is activated in a specific area depending on its locomotion abilities. The different platforms sweep the relevant metallic surfaces and grab video at a rate compatible with their speed. Images are transmitted to a control station to provide the surveyor with an overall view of the vessel's condition. Positioning information is also included with every image in order for the robots to be able to get to the same position/view later.

– *Stage B: Detailed video grabbing*. This stage is used by the surveyor for acquiring more detailed visual information from areas suspected from being affected by corrosion and/or cracks, and lasts up to the surveyor satisfaction. The robotic platforms are thus to resort to the previously gathered visual and positioning information to revisit the required hull areas.

– *Stage C: Thickness measurement*. At this moment of the mission, robots fitted with thickness measuring devices are deployed. Thickness measurements are taken at both the hull points specified by the Classification Society inspection rules and at the hull points suspected from being affected by a wastage level beyond allowable limits.

3.3. System architecture

The MINOAS architecture, as shown in Figure 2, consists of a hierarchical controller in charge of the dynamic task allocation among the team of heterogeneous robots, as well as handling the exchange of data with the fleet, and the related post-processing. Depending on the particular task to be undertaken, each kind of robot is to be fitted with a proper suite of sensors and actuators, although each platform is intended to be equipped with at least one camera to provide visual feedback of the area under inspection; special cameras, either infra-red or multi-spectral, if found useful, could also be incorporated.

The networking means required for this kind of scenario will not be restricted to wireless (ad-hoc) networks,

3

but will also be stretched out in adopting wired communication when the amount of transmitted data require large bandwidth, such as live video, or where the intervening physical mean does not allow for acceptable baud rates (underwater communication). In particular, a network monitoring system is to be developed for the online health monitoring of the network. This module will extract the coverage of the overall network and will locate blindfold regions, which should be avoided during the robot movements, or bridged to the network infrastructure in order to ensure accessibility. Widely acceptable metrics are to be used to evaluate the status of the ad-hoc networks (UDP based networks are susceptible to packet losses) and counter-measures will be taken to improve the network functionality (replacement of a malfunctioning stationary node with a mobile one).

Regarding the particular robotic platforms that are to account for the inspection missions: UAVs will be implemented through commercial VTOL (*Vertical Take-Off and Landing*) vehicles —quad-rotors to be more precise— fitted with the necessary payload, due to their suitability for both indoor and outdoor environments, while *Wall Climbers* will be developed from scratch as special platforms making use of magnetic locomotion. More details regarding the current state of development of the latter are given in Section 4.

Other issues such as robot localization, path planning or task allocation strategies specific for MINOAS are still matter of future research and will not be addressed here.

4. Magnetic wall climber

4.1. Application and system Requirements

To be useful in the application described above, the robot has to be simple and efficient. This implies a number of design requirements the platform has to fulfill: *mobility*, for the robot to be able to climb vertical metallic walls with a reasonable speed; *portability*, so that the robot is light enough to be carried by a single surveyor; *energy autonomy*, in order to avoid external power supplies involving cables and tethers; and *safe handling*, so that the robot, in absence of securing cables which would greatly limit its usability, is prevented from hurting the surveying personnel. A system design combining a light-weight minimalistic robot corpus with efficient wheel-based magnetic locomotion has been adopted to address these requirements.

4.2. Lightweight robot design

The current version of the light-weight inspection robot weights only 650 grams. This includes a Li-Io battery pack supporting energy autonomy for up to one hour, two high-performance Faulhaber electro-motors, electronics for motor control and communication, and a light-weight camera. This high performance-to-weight ratio has been achieved by using light-weight materials, such as Delrin plastic and fiberglass, for all the parts of the robot corpus.
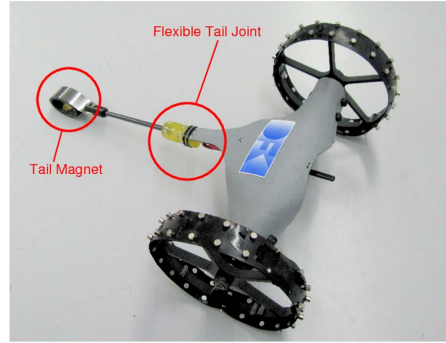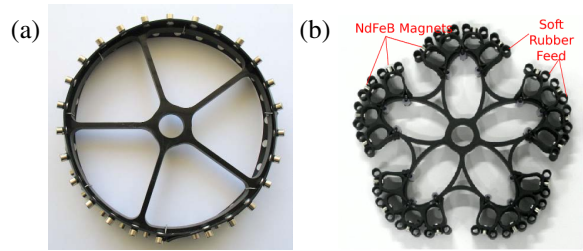

Figure 3. The flexible tail.

Figure 4. Wheel designs A and B.

Additionally, the design of the robot was simplified although preserving the fulfillment of the requirements. On the one hand, two wheels in cooperation with a flexible "tail" guarantee the stability of the system during rotation on the vertical wall (see Figure 3). On the other hand, each wheel is equipped with an individually controlled wheel-hub-engine, enabling high mobility and maneuverability.

4.3. Locomotion by magnetic wheels

Magnetic wheels have been used for efficient locomotion of the crawler on metallic surfaces. Compared to tracks, magnetic wheels have the advantage of being less complex. Furthermore, the use of light weight material (e.g. plastic) makes it possible to build a locomotion system that is much simpler and lighter than a tracked system. For the light-weight magnetic crawler, a combination of Delrin plastic, rubber and strong neodymium magnets are used to build a two-wheel locomotion system.

All wheeled or tracked magnetic crawlers have problems with small obstacles, including welds, bolts, or cables, which cause the loss of magnetic contact with the metallic surface and reduce or eliminate the traction of the robot. To overcome this problem, two different designs for magnetic wheels have been tested (see Figure 4): (1) wheel type A follows a standard wheel design, where traction is created by 50 high-power neodymium magnets embedded in a flexible rubber base; (2) wheel type B applies a hybrid wheel-leg design, where each wheel consists of five legs that end in a foot and each foot has a flexible rubber base with 8 high-power neodymium magnets.

In addition to the magnetic wheels, a strong neodymium magnet is included in the tail section. The passive but flexible magnetic tail proved to have a strong
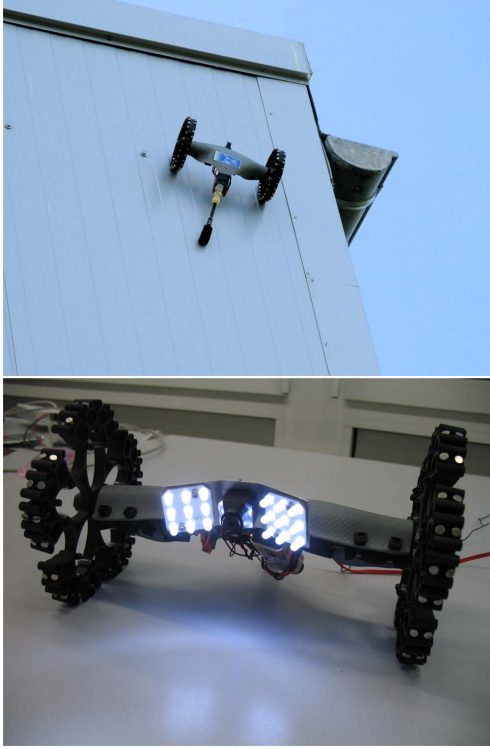
Figure 5. (top) Rear-view of the crawler in action. (bottom) Detail of the onboard camera and illumination system.

impact on the stability and maneuverability of the system.

To finish, Figure 5 presents the proposed crawler climbing up at a vertical metal test wall. For this experiment a round shaped wheel with magnets was used. The lower part of this figure also shows the wireless camera and LED-based light source fitted to the crawler.

5. Visual detection of defects

5.1. Crack detection

This section presents a crack detector based on a percolation model, as well as the algorithm by Yamaguchi and Hashimoto described in [8]. This latter method was, however, devised for detecting cracks in concrete, whose sinuous shape does not match the shape of cracks in steel, often shorter and thicker. Consequently, a new algorithm has been developed to cover the pattern corresponding to the steel case. It has also been extensively optimised to shorten the inspection time.

The percolation process consists in a region-growing procedure which starts from a seed element and propagates in accordance with a set of rules. In our case, the rules are defined to identify dark, narrow and elongated sets of connected pixels, which are then labelled as cracks. In order to optimize the detector, seed points are defined only at edges that have not yet been classified as crack pixels and whose gray level is below γ_s.

Once a seed has been located, the percolation process starts as a two-stage procedure: during the first stage, the percolation is applied inside a window of $N \times N$ pixels until the window boundary is reached; in the second step, if the elongation of the grown region is above ϵ_N, a second percolation is performed until either the boundary of a window of $M \times M$ pixels ($M > N$) is reached or the propagation cannot proceed because the gray level of all the pixels next to the current boundary are above the gray level of the seed pixel. Finally, all the pixels within the grown region are classified as crack pixels if the elongation is larger than ϵ_M. Elongation is calculated by means of $\epsilon = \sqrt{1 - R_{\min}/R_{\max}}$, where $R_{\min}$ and $R_{\max}$ are, respectively, the lengths of the short and long axes of the ellipse with the same area as the region [3].

Finally, at the end of the percolation process, the average gray level of the set of pixels is checked to determine if it is dark enough for the region to be considered as a crack, i.e. it is below a given threshold γ_a. Otherwise, the set of pixels is rejected and no labelling occurs.

Preliminary results for this algorithm are indicated superimposed in white over the original image in Figure 6(a, 2nd column). In all cases, $N = 51$, $M = 151$, $\gamma_s = \gamma_a = 0.3 \times 255$ and $\epsilon_N = \epsilon_M = 0.9$. As can be qualitatively observed, a high success rate is obtained for these images, although a reduced number of false positives coinciding with narrow shadows can also be noticed (see the image of the last row). Global percentages of false positives and false negatives, relative to image size, have been measured as, respectively, 2.29% and 0.47%.

5.2. Corrosion classifier

The corrosion detection approach has been built around a supervised classification scheme. The classifier makes use of a codeword dictionary computed during a previous learning stage. Each codeword consists of stacked histograms for the red, green and blue colour channels of image patches containing different kinds of rust (other colour spaces are under consideration). To reduce the dimensionality, intensity values are downsampled from 256 to 32 levels, and, thus, a codeword consists of 96 components.

For training, samples from essentially two different kinds of corrosion have been gathered: *general corrosion*, which appears as non-protective friable rust which can occur uniformly on uncoated surfaces, and *pitting*, a localized process that is normally initiated due to local breakdown of coating and that derives, through corrosive attack, in deep and relatively small diameter pits that can in turn lead to hull penetration in isolated random places. In order to make the dictionary more compact, codewords have been clustered, independently for every kind of rust considered, by means of the well-known K-means algorithm [7]. The size of the dictionary, i.e. the number of models, is therefore given by the number of clusters selected during the clustering process.

Once the dictionary has been built, the corrosion detector proceeds scanning the image and classifying every im-

(a) Crack detection

(b) Corrosion detection
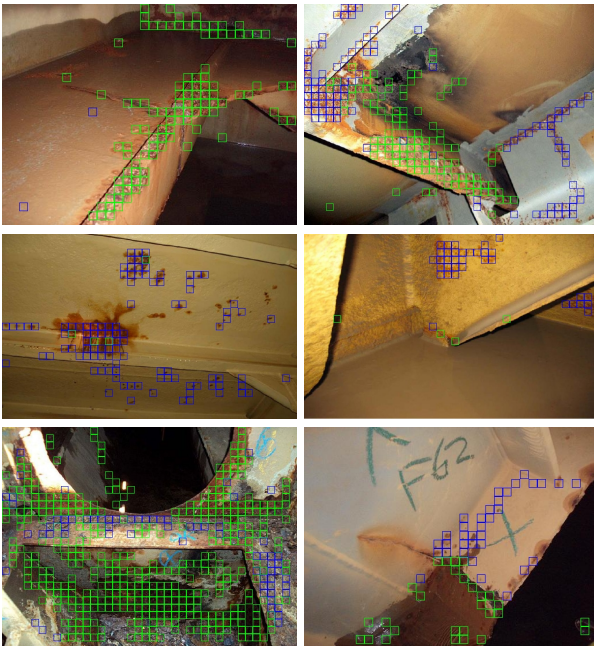
Figure 6. Preliminary results

age patch as affected by corrosion or not. To this end, the current patch codeword is built and compared with all the models of the dictionary by means of the Bhattacharyya distance $D = -\log(1 - B)$ [2], where B is given by Equation 1:

$$B = \int \sqrt{p_c(z)p_m(z)}dz\,, \qquad (1)$$

and p_c and p_m are histograms from, respectively, the codeword and the model. Using a nearest-neighbour rule, the closest model is selected and the patch is classified as corrosion only if $D < \tau_b$.

Preliminary results for this algorithm can be found in Figure 6(b), where the green and blue boxes correspond each to a different kind of corrosion. In all cases, the dictionary consisted of 50 models for every corrosion type and $\tau_b = 0.06$. As can be observed, the experiments performed indicate that, despite the loss of information due to the kind of codeword that has been defined, corrosion detection is attained at a reasonable level of performance.

6. Conclusions

First steps towards the automation of the visual inspection process of vessels have been described. Apart from presenting and justifying the interest of the whole project, this paper reports the design of a magnetic wall climber robot specially suited to this kind of environment, as well as promising results for the visual detection of defects by means of image processing techniques. Three key benefits are to be obtained from the visual detectors: (1) surveyors can use them to improve the targeting of their surveys by reliably identifying the areas where effort should be focused; (2) they provide consistency across surveyors, enabling them, regardless of location or training, to numerically quantify the amount of damage within a particular area; and (3) if employed frequently by ship owners, they can be used to quantify the progression of failures leading to preventive maintenance with reduced life-time costs.

References

[1] Remotely Operated Tanker Inspection System II (ROTISII). www.cybernetix.fr/Inspection-of-hulls. (15/07/2010).
[2] R. O. Duda, P. E. Hart, and D. G. Stork. *Pattern Classification, 2nd edition*. Wiley, 2001.
[3] B. Horn. *Robot Vision*. MIT Press, 1986.
[4] Lloyd's MIU. World merchant fleet.
[5] G. Meo and B. Papalia. The man-machine interface of RO-TIS ROV system. In *Proc. Oceans*, pages 1115–1120, 2001.
[6] S. Newsome and J. Rodocker. Effective technology for underwater hull and infrastructure inspection: The SeaBotix LBC. In *Proc. Oceans*, pages 1–6, 2009.
[7] S. Theodoridis and K. Koutroumbas. *Pattern Recognition, 3rd Edition*. Academic Press, 2006.
[8] T. Yamaguchi and S. Hashimoto. Fast crack detection method for large-size concrete surface images using percolation-based image processing (in press). *Machine Vision and Applications*, 2010.